Seismic Performance Evaluation of a High-Rise Building with Novel Hybrid Coupled Walls

Xiaodong Ji[1], Dan Liu[1] and Carlos Molina Hutt[2]

[1]*Department of Civil Engineering, Key Laboratory of Civil Engineering Safety and Durability of China Education Ministry, Tsinghua University, Beijing 100084, China*

[2]*Department of Civil Engineering, University of British Columbia, Vancouver, BC, Canada V6Z1Z4*

Abstract: In recent years, a novel type of hybrid coupled wall (HCW), which consists of reinforced concrete (RC) wall piers and replaceable steel coupling beams (RSCBs), has been proposed for enhancing the seismic resilience of high-rise buildings. This paper presents the assessment of the seismic performance of an 11-story building located in a highly seismic area and designed per modern Chinese codes. The building adopts the frame-shear wall interacting system. For comparison, two cases are considered: one using the novel hybrid coupled walls (HCW) and another using conventional RC coupled walls (RCW). The dynamic response of the buildings under high intensities of ground motion shaking is obtained from nonlinear dynamic analysis in OpenSees. The seismic performance, expressed in terms of repair cost and time, is assessed based on the FEMA P-58 method. The results indicate that most of the damage is concentrated in the coupling beams and nonstructural components. The use of novel HCWs instead of conventional RCWs results in the maximum interstory drift up to 24.5% lower in the HCW building than the RCW building when subjected to a maximum

considered earthquake (MCE) intensity. Novel HCWs result in a reduction of 50.8% and 60.5% in the median building repair cost and time, respectively, under MCE, due to less damage to coupling beams and RC frames and easy replacement of RSCBs after a damaging earthquake. It is also noted that HCWs have limited influence on the peak floor accelerations, and thus the repair cost and time for acceleration-sensitive non-structural components are similar for both the HCWs and the RCWs.

Keywords: hybrid coupled wall (HCW); replaceable steel coupling beam (RSCB); nonlinear dynamic analysis; seismic performance; high-rise building; non-structural components; seismic resilience.

1. Introduction

Recent major earthquakes including the 2010 Maule earthquake (Chile, Magnitude of 8.8), 2011 Tohoku earthquake (Japan, Magnitude of 9.0) and 2011 Christchurch earthquake (New Zealand, Magnitude of 6.3), have demonstrated that our built environment and infrastructure, particularly in the urban context, need to be more resilient to earthquakes. In order to ensure minimal disruption to everyday life and business in the urban society, prompt post-earthquake recovery of buildings is a clear need.

Coupled wall systems are often used in high-rise buildings due to their superior strength and stiffness. In such a system, coupling beams are designed to undergo inelastic deformation and dissipate seismic energy, as shown in Fig. 1. Once damaged, traditional reinforced concrete (RC) coupling beams are expensive and time-consuming to repair. As a result, various types of replaceable coupling beams have been recently proposed as an alternative to traditional RC coupling beams (e.g., Fortney et al. [1], Christopoulos et al. [2], and Ji et al. [3]). Among them, the replaceable steel coupling beam (RSCB), as shown in Fig. 4, appears to be very promising.

The RSCB comprises of a central “fuse” shear link connected to steel beam segments at its two ends. By means of capacity design principles, the inelastic deformation can concentrate in the “fuse” shear links, while the steel beam segments remain elastic. Extensive studies [4,5] have indicated that a short shear link with proper detailing can provide very stable and ductile behavior under cyclic shear loading. In addition, specialized link-to-beam connections have been developed which can ensure adequate shear and flexural strength of

the connections and allow the damaged shear link to be replaced easily, even in presence of residual drifts [3]. The RC slab above the RSCBs is elevated by a distance as proposed in [6]. Large-scale test results indicate that such 'isolated slab' has very limited influence on the initial stiffness, shear strength and hysteretic performance of the RSCB, and that damage to the slab is minimal even under an inelastic rotation of the coupling beam of 0.05 rad, thus enabling quick and easy repair. The RSCBs and RC wall piers form a novel hybrid coupled wall (HCW) whose superior structural performance against seismic action was demonstrated in a previous study [7].

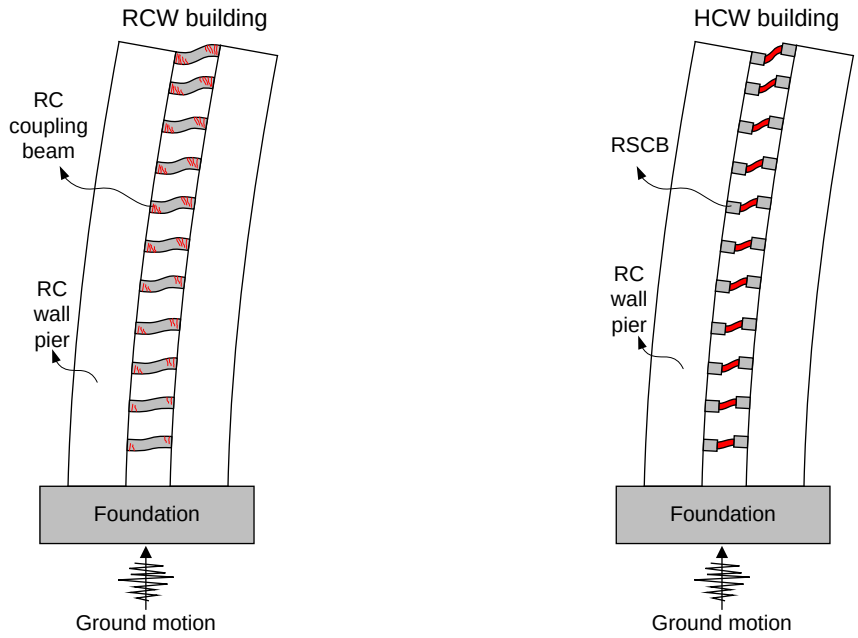

(a) RC coupled wall (b) Hybrid coupled wall

Fig. 1. Sketch of coupled walls

The objective of this paper is to evaluate the impact of adopting this novel HCW system on overall building performance, including damage to structural and non-structural systems, as well as post-earthquake repair cost and time. A realistic 11-story office building is considered for a case study. To illustrate the superior performance and benefit in reparability

of the high-rise building with HCWs using RSCBs (HCW building), its performance is compared against a building with commonly-used RC coupled walls (RCW building). To this end, Section 2 describes the structural design of the buildings considered. Section 3 presents the development of nonlinear numerical models and ground motion records selected for nonlinear dynamic analysis. Section 3 also summarizes global responses of the HCW and RCW buildings when subjected to high intensities of ground motion shaking. Section 4 assesses seismic performance of the buildings in terms of repair cost and repair time based on FEMA P-58.

2. Structural design

The prototype building is an 11-story office building located in Beijing, as shown in Fig. 2. It adopts a RC frame-shear wall interacting system. The total height of the structure is 48.5 m, and the plan dimension is 48.6 m by 14.4 m at the first floor, and 48.6 m by 17.65 m at other floors. The structural configuration and details of the prototype building are slightly modified from its as-built configuration, and are consistent with the representative floor plan shown in Fig. 2(b). The dead load of each floor including the self-weight of the floor slabs and the superimposed dead load varies from 5.5 kN/m^2 to 6.5kN/m^2. The live load is 2.5 kN/m^2.

(a) Photograph of prototype building under construction

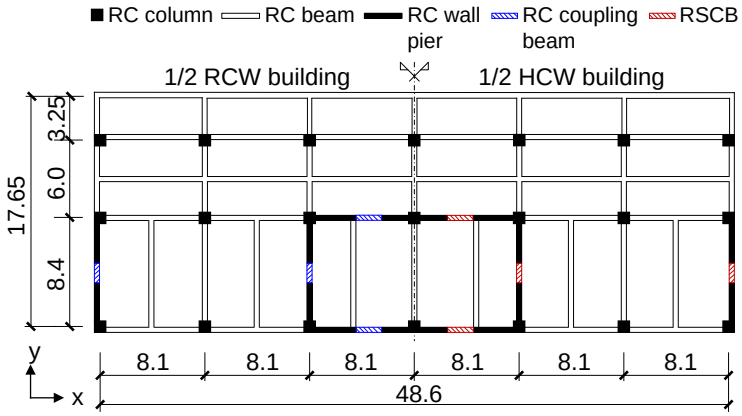

(b) Plan view (Units in m).

Fig. 2. Prototype structure

Based on the configuration of the prototype building, the structure is designed using HCWs according to the Chinese code for seismic design of buildings (GB 50011-2010) [8] and Chinese technical specification for concrete structures of tall buildings (JGJ 3-2010) [9]. The resulting dimensions of the beams in the frame are 250 × 700 mm, and the dimensions the columns range from 700 × 700 mm to 900 × 900 mm. The thickness of shear walls is 300 mm. Linear response spectrum analysis of a three-dimensional structural model is performed

to determine the design forces of the structural components and the deformation of the structure under service level earthquake (SLE, with a probability of exceedance of 63% in 50 years), which has a peak ground acceleration (PGA) of 0.07 g. In this analysis, a damping ratio of 5% is assumed for all modes, and accidental eccentricity of 5% is considered in each direction to account for torsional effects. In accordance with GB 50011-2010, the elastic stiffness E_cI_g is used for the RC wall piers and columns, as their deformations are very small under SLE (interstory drift ratio limit of 1/800). The stiffness of RC frame beams is taken as 1.5 E_cI_g (for exterior beams) or 2.0 E_cI_g (for interior beams), to account for the increased stiffness associated with the RC slabs above the beams. The structure is designed as a dual system, and the design shear force for the RC frames in each floor is adjusted to be over $0.2V_0$ or $1.5V_{fmax}$ in accordance with GB 50011-2010 [8], where V_0 denotes the calculated total base shear force and V_{fmax} denotes the maximum value of the calculated floor shear force in the RC frames across all stories.

The first three natural periods of the HCW building are 1.31 s, 1.20 s and 1.00 s, corresponding to the vibration modes of translation in the *x* direction (i.e., longitudinal direction), translation in the *y* direction (i.e., transverse direction) and the torsional mode, respectively. Fig. 3 shows the interstory drift ratios and shear-to-gravity coefficients of the structure under SLE. Note that the shear-to-gravity coefficient of a story denotes the ratio of the shear force of the story over all the gravity loads above this floor. The maximum interstory drift ratio is less than the upper limit 1/800 required in GB 50011-2010 [8], and the minimum shear-to-gravity coefficients is larger than the lower limit of 0.032 [8].

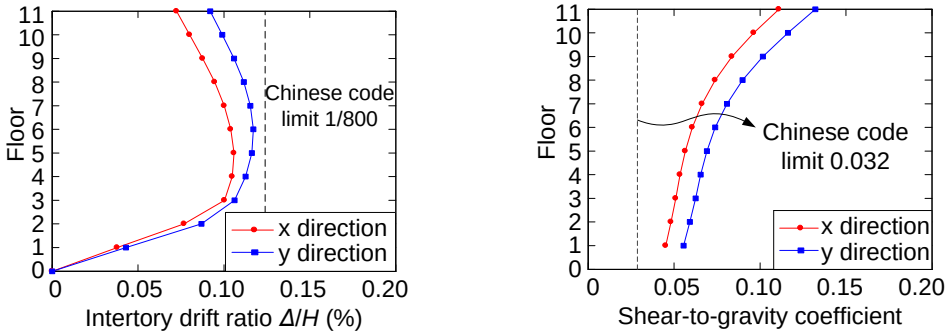

(a) Interstory drift ratio (b) Shear-to-gravity coefficient

Fig. 3. Elastic analysis results under SLE

Per the Chinese code requirements, structural components are designed to satisfy the strength demand under SLE, and proper ductile detailing is provided to enable the development of plastic deformations under maximum considered earthquake (MCE, with a probability of exceedance of 2% in 50 years) shaking. Concrete with a strength grade of C35 (nominal cubic compressive strength f_{cu} = 35 MPa, and nominal axial compressive strength f_{ck} = 23.4 MPa) and HRB400 steel reinforcement (nominal yield strength f_y = 400 MPa) are used in the beams. C45 concrete (f_{cu} = 45 MPa, f_{ck} = 29.6 MPa) and HRB400 rebars are used in columns and wall piers. The frames are designed to satisfy the "strong column-weak beam" requirement. The wall piers are design with well-detailed boundary elements per the GB 50011-2010 provisions to ensure their ductile response. The reinforcement details of the structural components can be found in Reference [10].

Fig. 4 shows a representative RSCB of an exterior HCW in the *y* direction. The RSCB consists of a "fuse" shear link at the mid-span and two steel beam segments that connect the ends of the shear link to the walls. Both the shear link and the beam segments adopt built-up I-shaped steel sections. A hybrid section is used for the link, where the link flanges are made of Q345 steel (f_y = 345 MPa) and the link webs of Q235 steel (f_y = 235 MPa). The links are

designed in a shear yielding mode, with a length ratio $e/(M_p/V_p)$ ranging from 0.63 to 0.91. Note that e denotes the length of shear link, and M_p and V_p denote the plastic flexural strength and shear strength of the link, respectively. The steel beam segments are made of Q345 steel. To ensure that the beam segments remain elastic, their strength is designed to exceed the overstrength of the shear link. The overstrength factor Ω of the shear link with a length ratio less than 1.0 is taken as 1.9 as suggested by Ji et al. [5]. The shear link is connected to the beam segments using an end-plate connection with high-strength bolts and shear keys, as shown in Fig. 4. The performance and replaceability of this type of link-to-beam connections is described in Ji et al. [3].

The RSCBs are connected to the wall piers through an embedded connection detail, as shown in Fig. 4. The embedded beam-wall connection design complies with the requirements for steel coupling beams in AISC 341-10 [11], where the embedded length is sufficient to develop an adequate beam-to-wall pier strength exceeding the overstrength of the shear links. Furthermore, the face bearing plates and transfer bars are used to ensure the stiffness and ductility of the joint.

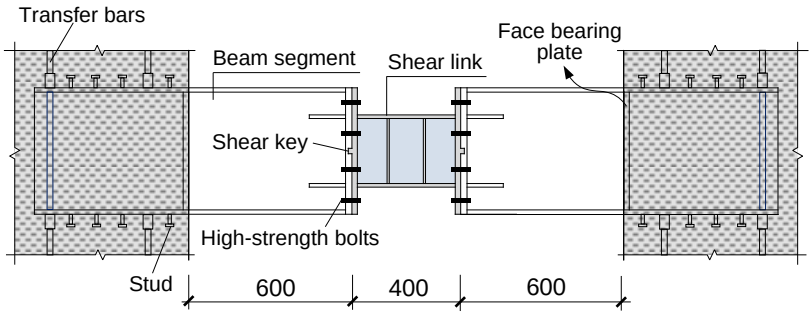

Fig. 4. Replaceable steel coupling beam (units in mm).

A structure with conventional RC coupling beams is also designed for comparison against the HCW structure with RSCBs. The RC coupling beams are designed to have nearly

identical nominal shear strengths and effective stiffness as the RSCBs. Note that the effective flexural stiffness of RC coupling beams is taken as $0.15E_cI_g$, as recommended by Naish et al. [12]. Design results of other structural components in the RCW building are exactly the same as those in the HCW building. Therefore, the calculated values of dynamic properties and structural responses under SLE of the RCW building are nearly identical to those values of the HCW building.

3. Nonlinear response time history analysis

3.1. Numerical model

Three-dimensional numerical models of the HCW structure and the RCW structure are developed in OpenSees [13]. Fig. 5 shows numerical models for wall piers and frame components. The multi-layer shell element [14] is adopted for modeling of the RC wall piers. In the multi-layer shell element, concrete is represented by a number of concrete layers, and the distributed reinforcement is represented by smeared rebar layers. The longitudinal rebars in the boundary elements are modeled with truss elements, and they are coupled with the surrounding shell elements by coupling the degrees of freedom (DOFs) at the coincident nodes. The fiber beam-column element is adopted to model columns and beams in the frames. A frame beam or column member is divided into five beam-column elements, and each element includes three integration points. The frame beam and column are rigidly jointed to each other at the intersection point of their center lines. For the wall piers and frame elements, the concrete cover is represented by the Kent-Park model [15]. In this model, the stain at the peak stress is assumed to be 0.002, and the residual compressive strength after ultimate strain

is assumed to be 0.2 times the peak strength of the unconfined concrete. The stirrup-confined concrete is represented by the Saatcioglu-Razvi model [16], which takes into account the increase of the strength and ductility of concrete due to confinement effect. The residual compressive strength after ultimate strain is assumed to be 0.2 times the peak strength of the confined concrete. The uniaxial tensile stress-strain relationship of concrete is represented by a bilinear curve, which takes into account the tension softening and the ultimate tensile strain, which is assumed to be 0.001. The Giuffré-Menegotto-Pinto model [17] is adopted to represent the uniaxial stress-strain relationship of the steel reinforcement. In this model, the strain-hardening ratio after yielding is assumed to be 1%. The parameters R0, CR1 and CR2, which control the curve shape of the transition from elastic to plastic branches are taken as 18.5, 0.925 and 0.15. The models for wall piers, frame columns and beams have been validated with test results, as detailed in References [18,19].

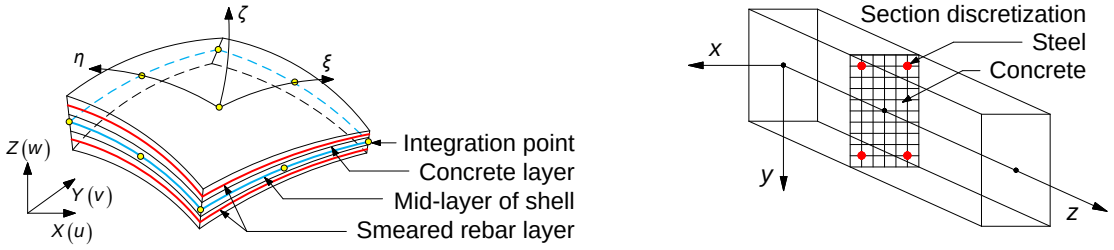

(a) Multi-layer shell element [14]

(b) Beam-column element with fiber section [19]

Fig. 5. Sketch of elements for RC walls and frame components.

Fig. 6 shows the simplified numerical model for the RSCBs. The shear link is simulated by a nonlinear link element. The mechanical behavior on each degree of freedom is modeled by a user-defined spring. In this case, the shear link is designed to yield in shear. Therefore the axial spring and flexural spring are elastic, while the shear spring is nonlinear. The beam

segment is designed to remain elastic under seismic action, and thereby it is modeled by an elastic beam element in OpenSees. This beam element does not include shear deformation, but shear deformation of short-span beam segments is not negligible. Therefore, a zero-length shear spring element is set between the beam element and the link element, for representing the shear stiffness of beam segment. RC coupling beams are modeled with a nonlinear link element. The skeleton of the force-displacement relationship is defined following the ASCE/SEI 41-13 provisions [20], and the parameters of hysteretic model are calibrated with test results. More details of the OpenSees models and associated parameters for RSCBs and RC coupling beams can be found in [7]. These models have been validated with the test data [7].

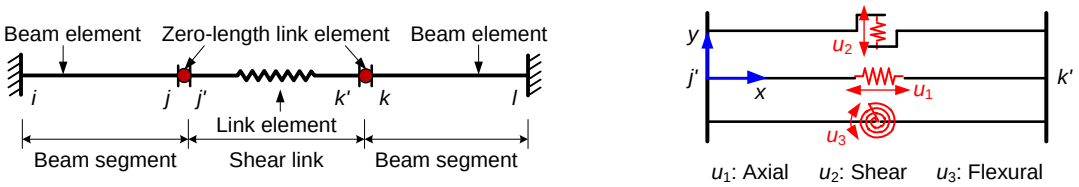

(a) Coupling beam model (b) Link element

Fig. 6. Nonlinear model for RSCB.

3.2. Ground motions and nonlinear dynamic analysis parameters

According to GB 18306-2015 [21], the peak ground acceleration (PGA) at the site of the prototype building under MCE shaking is 0.4 g. The amplitudes of the very rare earthquake (VRE, with a probability of exceedance of 0.5% in 50 years) is 1.5 times that of the MCE. The site of the prototype building falls into Site Class III, with an average shear wave velocity in the top 30 m of soil, V_{S30}, between 150 m/s and 250 m/s. The characteristic period of the seismic response spectra, T_g, is 0.45 s.

Seven bi-directional ground motion records are selected from the NGA West 2 Ground Motion Database [22]. The target spectrum is the MCE response spectrum, and the linear scaling method is used in the ground motion selection procedure. Record characteristics with magnitudes greater than 6, average shear wave velocity consistent with Site Class III and no restriction on fault type and fault distance are used to search the database for selecting records to match the target spectrum over the period range of interest. The selected ground motion records, geomean of each pair of individual record spectra, the mean spectrum of the selected records and the target spectrum plotted against the period range of interest are shown in Fig. 7.

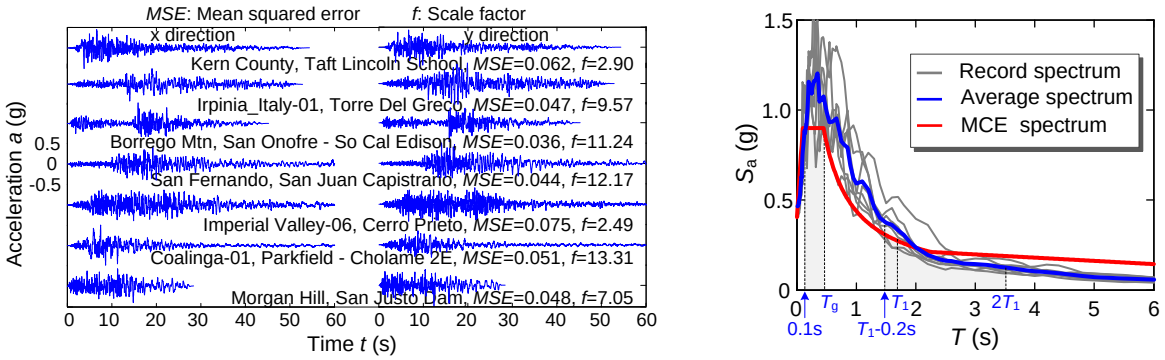

(a) Acceleration time histories of scale motions at MCE

(b) Target spectra and response spectra of scaled motions at MCE

Fig. 7. Selected ground motion records and response spectra.

The selected ground motions are input at the base of the structures, which are assumed to be fixed at their base. Following the recommendations in GB 50011-2010 [8], a damping ratio of 5% is assumed in the analysis, implemented using the Rayleigh damping model for the 1st and 9th vibration modes of the structures (i.e., the first three modes in each direction of translational vibration and torsional vibration). The Newmark-β method is adopted to solve the integration of differential equations, and the Newton-Raphson algorithm is used to solve

the nonlinear residual equation.

3.3. Dynamic analysis results

Fig. 8 compares the time histories of roof drift of the HCW building and the RCW building in *y* direction when subjected to the Coalinga-01 motion at VRE. Within the first 6 seconds, the HCW and the RCW structures remain elastic, and the time history responses of both structures are nearly identical. After 6 seconds, the structures yield, and the time history responses of the two buildings diverge. In general, the responses of the HCW structure appear to have a higher frequency and faster rate of decay of vibration relative to those of the RCW structure, indicating that, in the plastic region, the former has larger equivalent lateral stiffness and higher equivalent hysteretic damping than the latter.

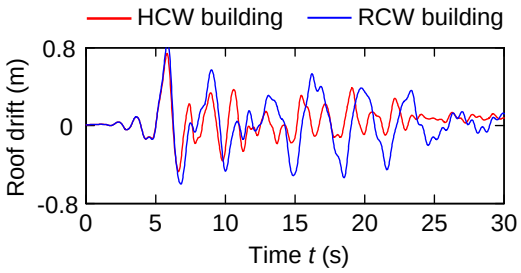

Fig. 8. Time histories of the responses of HCW and the RCW buildings at VRE.

Fig. 9 compares the maximum interstory drift ratios at each floor of the HCW building and the RCW building. The maximum interstory drift ratio of the HCW building is up to 24.5% smaller at MCE and 32.7% smaller at VRE than the RCW building. When subjected to severe earthquakes, the RSCBs have stable hysteretic responses and achieve large overstrengths in the cyclic reversal after yielding of the shear links (see Fig. 10), which ensures an adequate coupling ratio. On the contrary, the conventional RC coupling beams have considerable degradation of stiffness and strength after yield, which in turn leads to a

decrease in the coupling ratio of the coupled wall system. The variation in coupling ratios is the major reason why the HCW building shows smaller interstory drifts than the RCW building under MCE and VRE. In addition, the greater energy dissipation capacity of the RSCBs versus the RC coupling beams can further decrease the lateral drifts of the HCW building.

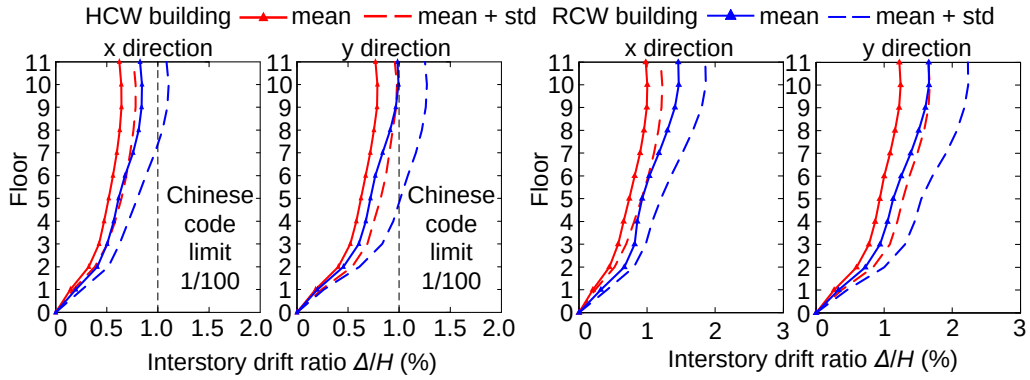

(a) MCE (b) VRE

Fig. 9. Interstory drift ratios of the HCW and the RCW buildings.

Fig. 10 compares the maximum floor accelerations of the HCW building and the RCW building. The distribution of the maximum floor accelerations highlights the contribution of high modes to the acceleration response. The floor accelerations of both HCW and RCW buildings are of similar magnitude, indicating that use of HCWs is likely to have limited influence on suppressing floor accelerations.

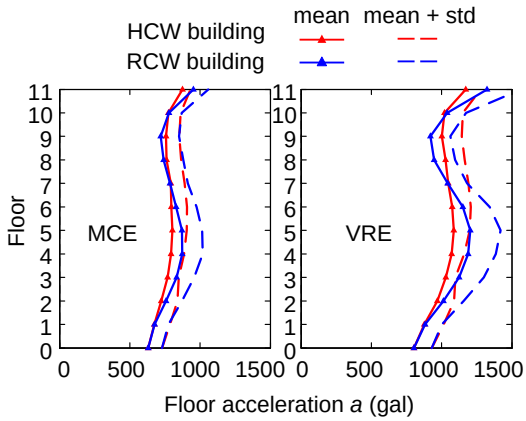

Fig. 10. Floor accelerations of the HCW building and the RCW building.

4. Assessment of seismic performance

4.1. Fragility and consequence functions of structural components

Performance-based seismic design is a formal design process for new buildings or retrofit of existing buildings, with a specific intent to achieve a pre-defined performance objective in future earthquakes. Optimal methods have been developed for the performance-based seismic design [23, 24, 25]. In the next-generation of performance-based seismic assessment guidelines of FEMA P-58 [26], seismic performance is expressed as the probable consequences in terms of repair cost and repair time associated with a certain intensity of ground motion shaking. In this paper, the seismic performance of the HCW and the RCW buildings under MCE and VRE is assessed based on the FEMA P-58 methodology. In this procedure, component damage assessment relies on fragility data of the individual building components. A component fragility function is a statistical distribution that indicates the conditional probability of incurring damage at a given value of engineering demand parameter (EDP), which is typically assumed to be lognormal distribution. FEMA P-58 developed fragility functions for different kinds of components based on experimental data from the U.S. However, due to the difference in seismic design requirements and detailing between Chinese

codes and U.S. codes, the fragility functions of FEMA P-58 might not be applicable for structural components designed per Chinese codes.

Ji et al. [27] developed fragility functions for wall piers and RC coupling beams conforming to Chinese codes. Experimental data of 87 slender shear wall specimens and 36 conventional RC coupling beam specimens are collected, and design details of all the specimens are checked to ensure conformance with the requirements of the Chinese code. Table 1 and 2 compare the fragility functions developed by Ji et al. with those by FEMA P-58. The results show that RC wall piers designed per Chinese codes have smaller deformation capacity than those values specified in FEMA P-58, because the Chinses code requirements for the length of the special boundary element and the amount of boundary transverse reinforcement are lower than those requirements in the U.S. ACI 318-14 code. The medium values of fragility functions for conventional RC coupling beams developed by Ji et al. are quite smaller than those specified in FEMA P-58. Such difference might result from the variety in test data bases, as the FEMA P-58 develops the fragility curves for conventional RC coupling beams based on very limited test data. In this paper, the fragility functions developed by Ji et al. are used in the performance assessment.

Table 1. Fragility data of slender RC wall from Ji et al. [27] and FEMA P-58 [26].

Damage state	Damage description	Repair method	Fragility data	
			Ji et al.	FEMA P-58
DS1	Initial cracking	Cosmetic repair of surface finish	Median: 0.15% Dispersion: 0.58	Median: 0.11% Dispersion: 0.79
DS2	Cover spalling	Epoxy injection and patching cover	Median: 0.81% Dispersion: 0.27	Median: 0.90% Dispersion: 0.51
DS3	Exposure of rebar	Replacement of damaged concrete	Median: 1.10% Dispersion: 0.21	Median: 1.19 % Dispersion: 0.41
DS4	Concrete crushing and rebar buckling	Replacement of the wall	Median: 1.34% Dispersion: 0.30	Median: 1.86% Dispersion: 0.43

Notes: The engineering demand parameter used in the assessment of RC wall piers is drift ratio.

Table 2. Conventionally reinforced coupling beam fragility data from Ji et al. [27] and FEMA P-58 [26].

Damage state	Damage description	Repair method	Fragility data	
			Ji et al. $1.0 < l/h < 2.5$	FEMA P-58 $1.0 < l/h < 2.0$
DS1	Initial cracking	Epoxy injection	Median: 0.48 % Dispersion: 0.47	Median: 1.37 % Dispersion: 0.21
DS2	Cover spalling	Epoxy injection and patching cover.	Median: 1.04 % Dispersion: 0.37	Median: 2.64 % Dispersion: 0.33
DS3	Concrete crushing and rebar buckling	Replacement of coupling beam	Median: 2.36 % Dispersion: 0.37	Median: 4.28 % Dispersion: 0.74

Notes: l and h denote length and depth of coupling beam, respectively. The engineering demand parameter used in the assessment of the coupling beam is the chord rotation.

Consequence functions are required for assessment of repair cost and repair time based on component damage assessment results. A consequence function is a statistical distribution that indicates the conditional probability of a performance measure at a given damage state. Consequence functions, as provided by FEMA P-58, are used in this study, as the

consequence functions have yet to be developed in Chinese design guidelines. While the resulting repair cost and time (in absolute terms) are not directly applicable to the Chinese context, they enable a comparison of the relative improvement in performance between the HCW and the RCW systems in a high-rise building.

The RSCB is an innovative structural component. As a result, no fragility or consequence functions for RSCBs are available in the database developed for the FEMA P-58 project. Based on a volume of experimental data of very short links and RSCB specimens, Ji et al. [6] developed fragility functions for RSCBs. This research developed consequence function for RSCB based on the same experimental data. The consequence functions are developed using FEMA P-58 Consequence Estimation Tool to be consistent with US practice. The consequence functions are developed based on a detailed description of the repair scope associated with each damage state, including actual damage and collateral work (e.g. removal and replacement of finishes). Consequence data (repair techniques and cost estimates) available through the FEMA P-58 fragility function database are utilized as they apply to the RSCB components. Median values of repair cost and time are developed for each damage state accounting for economies of scale. A dispersion of is then assigned, based on judgement, to account for uncertainty in the median estimates. The parameters that define the fragility and consequence functions are summarized in Table 3. The parameters in consequence functions are described in Fig. 11.

Table 3. RSCB fragility and consequence function data.

Damage state	Damage description	Repair method	Fragility data [**Error! Bookmark**	Consequence function data		
				Quantity	Repair Cost ($)	Repair time (day)

not defined.]

DS1	RC slab damage	Epoxy injection and patching cover	Median: 5% Dispersion: 0.30	Min: 2 Max: 5	Min: 16712 Max: 25068 β: 0.31	Min: 10.00 Max: 15.00 β: 0.40
DS2	Link web or flange buckling	Heating or replacing shear link	Median: 9% Dispersion: 0.19	Min: 2 Max: 5	Min: 18357 Max: 27535 β: 0.27	Min: 11.04 Max: 16.55 β: 0.37
DS3	Link facture	Replacement of shear link	Median: 11% Dispersion: 0.15	Min: 2 Max: 5	Min: 18357 Max: 27535 β: 0.27	Min: 11.04 Max: 16.55 β: 0.37

Notes: RSCBs' EDP is shear link rotation. β denotes dispersion.

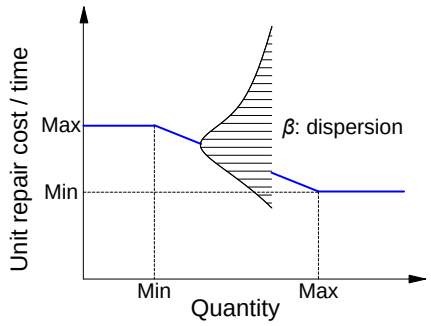

Fig. 11. Parameters of consequence functions [26].

As fragility and consequence data for frame components and non-structural components has not been developed yet in China, the data recommended in FEMA P-58 is used in the performance assessment of these components.

4.2. Performance model of buildings

The building performance model is an organized collection of data used to define the building assets that are vulnerable to the effects of earthquake shaking. The quantities and distribution of vulnerable structural components in the prototype buildings are shown in Table 4.

Table 4. Fragility groups of structural components.

Building	Component	Fragility member	Unit	Quantity		EDP
				x	y	

HCW & RCW	Frame joint	B1041.001a (FEMA P-58)	1 EA	10	14	IDR
		B1041.001b (FEMA P-58)	1 EA	9	3	IDR
	RC shear wall	RC Wall (Table 1)	144 SF	10.00	11.14	Harmful IDR
HCW	RSCB	RSCB (Table 3)	1 EA	4	4	Link rotation
RCW	RC coupling beam	RCCB (Table 2)	1 EA	4	4	Beam rotation

Notes: RCWall, RSCB and RCCB are user-defined fragility groups. The quantity in the table is the amount of components on one floor. EDP denotes engineering demand parameter. IDR denotes interstory drift ratio. EA denotes each. SF denotes square feet.

Different components are sensitive to different engineering demand parameters (EDP). EDPs for RC coupling beams, RSCBs and frames are beam rotation, shear link rotation and interstory drift ratio respectively. For the damage assessment of wall piers, simply using interstory drift ratio as EDP is no appropriate. On the upper floors of the buildings considered, rigid body rotation contributes to a large portion of the interstory drift ratio. However, this mode of deformation does not cause damage to the wall piers. Therefore, the harmful interstory drift ratio, which removes the effect of rigid rotation, as suggested by Cai et al. [28], is a better proxy for damage as hence used as EDP. The calculation of harmful interstory drift ratio is illustrated in Fig. 12.

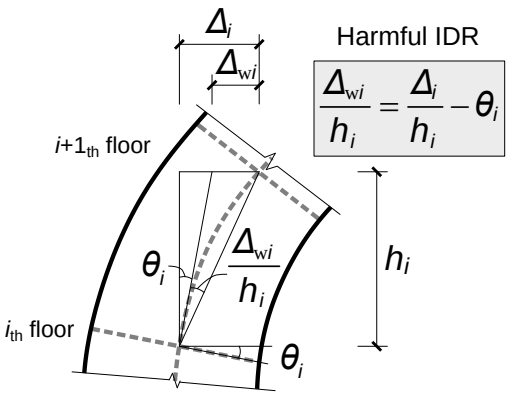

Fig. 12. Calculation of harmful interstory drift ratios of wall piers.

Non-structural components in the HCW and RCW buildings are assumed to be the same. The quantities and distribution of vulnerable structural components are estimated using the FEMA P-58 Normative Quantity Estimation Tool for an office building, as shown in Table 5.

Table 5. Fragility groups of non-structural components.

Category	Component	Fragility number	Unit	Floor	Quantity	EDP
Façade	Curtain walls	B2022.032	30 SF	2-11	92.33(#)	IDR
Fitout	Wall partition	C1011.001a	100 LF	2-11	9.23(#)	IDR
	Wall partition finishes	C3011.001a	100 LF	2-11	0.70(#)	IDR
	Raised access floor	C3027.001	100 SF	2-11	69.25(#)	A
	Suspended ceiling	C3032.001a	250 SF	2-11	33.24(#)	A
	Independent pendant lighting	C3034.001	1 EA	2-11	138.50(#)	A
Egress	Traction elevator	D1014.011	1 EA	1	3	A
	Concrete stairs	C2011.011b	1 EA	1-11	1	IDR
Plumbing	Potable water piping	D2021.011a	1000 LF	2-11	0.14(#)	A
	Hot water piping	D2022.011a	1000 LF	2-11	0.78(#)	A
		D2022.021a	1000 LF	2-11	0.28(#)	A
	Sanitary waste piping	D2031.011b	1000 LF	2-11	0.53(#)	A
	Fire sprinkler water piping	D4011.021a	1000 LF	2-11	1.85(#)	A
	Fire sprinkler drop	D4011.031a	100 EA	2-11	0.83(#)	A
HVAC	Chiller	D3031.011a	75 TN	11	4	A
	Cooling tower	D3031.021a	75 TN	11	4	A
	HVAC ducting	D3041.011a	1000 LF	2-11	0.69(#)	A
		D3041.012a	1000 LF	2-11	0.18(#)	A
	HVAC drops / diffusers	D3041.031a	10 EA	2-11	8.31(#)	A
	Variable air volume box	D3041.041a	10 EA	2-11	6.46(#)	A
	Air handling unit	D3052.011a	4000 CF	11	18	A
Electrical	Motor control center	D5012.013a	1 EA	11	4	A
	Low voltage switchgear	D5012.021a	225 AP	1-11	1	A
	Distribution panel	D5012.031a	1 EA	1-11	1	A

Notes: The quantity in the table is the amount of components on one floor. The value marked with (#) is the component quantity on floor 2 to 11, the component quantity on floor 1 is 0.816 times the marked value. EA denotes each. LF denotes linear fee. SF denotes square feet. CF denotes cubic feet. TN denotes ton. AP denotes ampere. EDP denotes engineering demand parameter. IDR denotes interstory drift ratio. A denotes acceleration.

4.3. Assessment results

4.3.1 Repair cost

Seismic performance prediction program (SP3), which implements the FEMA P-58 method, is used to carry out the probabilistic calculations associated with the seismic

performance of the buildings under consideration. Building collapse is not included in the analysis as the nonlinear dynamic response indicates that there is a negligible probability of collapse even under VRE (none of the analysis simulations result in collapse). Furthermore, the damage estimates indicate that the RC shear walls only experience slight damage (DS1) in the lower stories under VRE. The RC frames sustain slight damage (DS1) in most stories and only a few RC frames in the upper stories suffer moderate damage (DS2). Such damage of the gravity load-carrying components is unlikely to result in the collapse of buildings.

Even though the potential for excessive residual drifts rendering the building irreparable are considered, due to limited permanent deformations in the archetype buildings, these do not contribute to the expected losses. Fig. 13 shows the resulting performance functions for repair cost. The repair cost coefficient is the ratio of repair cost to total replacement cost. The total replacement cost is estimated at $29.86 million US dollars, based on the gross square footage and a rate of $299 per square foot. The mean repair cost of the HCW building is 50.8% lower at MCE and 41.9% lower at VRE than that of the RCW building.

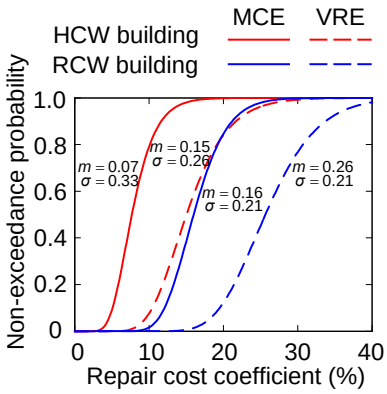

Fig. 13. Performance functions of repair cost.

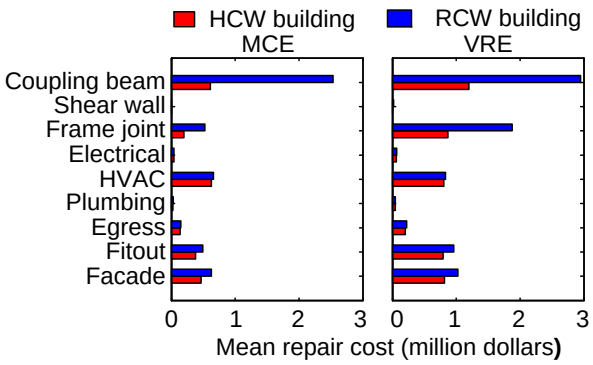

Fig. 14. Mean repair cost by component category.

Fig. 14 shows mean values of repair costs by component category. In the RCW building,

RC coupling beams account for 50.9% at MCE and 36.7% at VRE of the total repair cost, and frames account for 9.3% at MCE and 24.0% at VRE of the total repair cost. The implementation of HCWs in the building efficiently reduces damage in coupling beams and frames, which leads to significant reductions of the corresponding repair cost. In the RCW building, non-structural components account for around 40% of the total repair cost at MCE and VRE, which is similar to the estimated percentage value for a 40-story RC core building by Yang et al. [29]. Most damage to the non-structural components in the estimated buildings are sensitive to floor acceleration. The repair cost of non-structural components in the HCW building is only slightly smaller than those of the RCW building because HCWs are limited in their ability to reduce peak floor accelerations.

Fig. 15 shows the distribution of mean values of floor repair cost along the building height. Story repair cost increases with the increasing height, because the interstory drifts and coupling beam rotations are larger in the upper stories, which leads to more severe damage to frames and coupling beams. A significant increase of repair cost in the top story is caused by severe damage to a large number of HVAC components that are located atop the building. Repair cost associated with egress is noted in the first story because the FEMA P-58 fragilities for elevators were developed based on empirical observations of damage to elevator systems expressed as a function of peak floor acceleration at the base of the buildings.

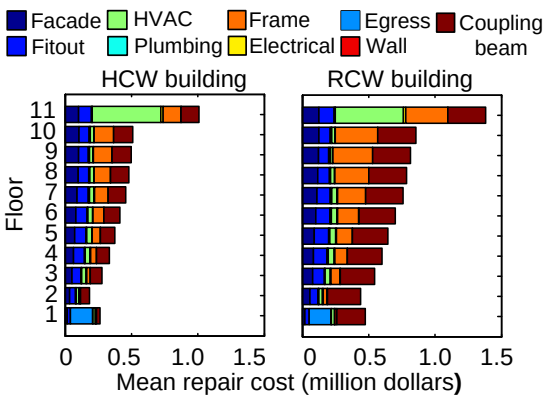

Fig. 15. Distribution of mean story repair cost along the height at VRE

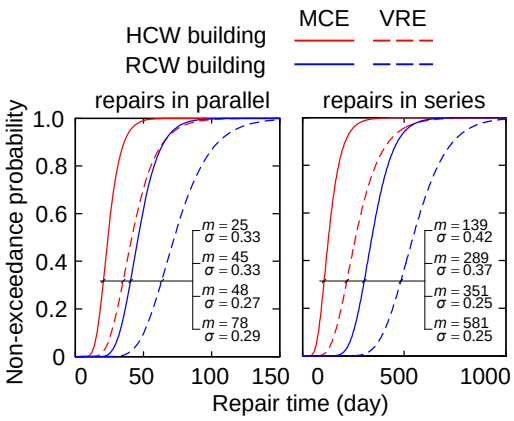

Fig. 16. Performance functions of repair time

4.2.1 Repair time

Fig. 16 shows the assessment results of repair time. There are two methods to calculate the repair time. One method assumes that all stories are repaired simultaneously (noted repair in parallel), and thus the repair time of a building is governed by the maximum story repair time. The other method assumes that each story is repaired sequentially (noted repair in series), and the repair time of the building is the sum of repair time of all stories. The sequential repair time, which reflects the total repair work, is 60.5% shorter at MCE and 50.4% shorter at VRE in the HCW building than the RCW building.

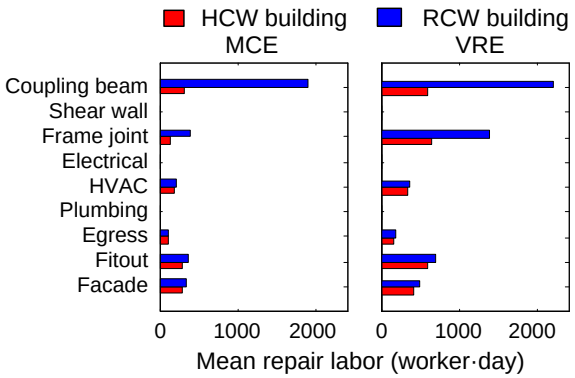

Fig. 17. Mean repair labor by component category

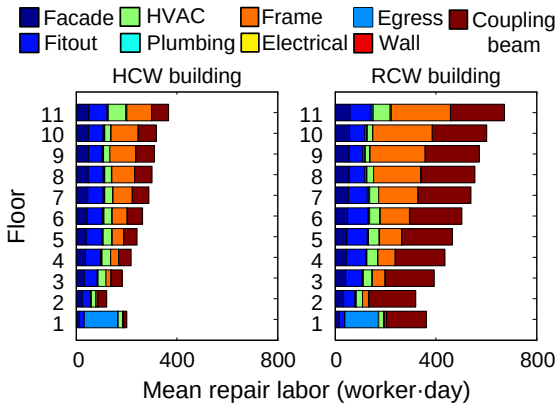

Fig. 18. Vertical distribution of mean floor repair labor at VRE

Fig. 17 shows mean values of repair labor by component category. One unit of repair

labor equals to one day of work of one worker. In the RCW building, the repair labor of structural components accounts for around 68% of the total labor under MCE and VRE. The use of RSCBs enables easy repair of coupling beams and reduce damage to the frames, thus leading to a significant decrease in repair labor. Fig. 18 shows the distribution of story repair labor along the building height. Similar to the distribution of repair cost, story repair time increases with the increasing height, as the interstory drifts and coupling beam rotations are larger in the upper stories.

5. Conclusions

A novel type of hybrid coupled wall (HCW), which consists of reinforced concrete (RC) wall piers and replaceable steel coupling beams (RSCBs), was proposed for enhancing the seismic resilience of high-rise buildings. This study assesses the seismic performance of a HCW building at high intensity levels of ground motion shaking as defined in the Chinese code: maximum considered earthquakes (MCE) and very rare earthquakes (VRE). The performance of the HCW building is compared against an equivalent RCW building with RC coupled walls (RCW).

Nonlinear numerical models are developed in OpenSees for a representative 11-story building located in Beijing and designed per modern Chinese standards. The nonlinear dynamic analysis indicates that use of novel HCWs instead of conventional RCWs leads to the maximum interstory drifts 24.5% lower at MCE and 32.7% lower at VRE in the HCW building than the RCW building. However, the use of novel HCWs has limited influence on maximum floor accelerations.

A seismic performance assessment of the buildings is carried out to estimate repair cost and repair time based on the FEMA P-58 method. Under MCE and VRE, in the RCW building, RC coupling beams and frames greatly contributes to the repair cost, while the HCW building efficiently controls damage in coupling beams and frames. The resulting repair cost of the HCW building is 50.8% lower at MCE and 41.9% lower at VRE than that of the RCW building. Due to the easy replacement of damaged shear links in RSCBs, the HCW building shows enhanced performance, particularly with regards to reductions in repair time. The repair time of the HCW building is 60.5% lower at MCE and 50.4% lower at VRE than that of the RCW building.

Acknowledgments

The work presented in this paper was sponsored by the International Science & Technology Cooperation Program of China (Grant No. 2014DFA70950) and the National Natural Science Foundation of China (Grants No. 51261120377 and No. 51678347). The authors wish to express their sincere gratitude to the sponsors.

References

[1] Fortney P J, Shahrooz B M, Rassati G A. Large-scale testing of a replaceable “fuse” steel coupling beam. J Struct Eng, ASCE 2007; 133(12): 1801-7.

[2] Christopoulos C, Montgomery M. Viscoelastic coupling dampers (VCDs) for enhanced wind and seismic performance of high-rise buildings. Earthquake Eng Struct Dynam 2013; 42(15):2217–33.

[3] Ji X, Wang Y, Ma Q, Taichiro O. Cyclic behavior of replaceable steel coupling beams. J

Struct Eng, ASCE 2017; 143(2): 04016169.

[4] Okazaki T, Arce G, Ryu H C, Engelhardt M D. Experimental study of local buckling, overstrength, and fracture of links in eccentrically braced frames. J Struct Eng, ASCE 2005; 131(10): 1526-35.

[5] Ji X, Wang Y, Ma Q, Okazaki T. Cyclic behavior of very short steel shear links. J Struct Eng, ASCE 2016; 142(2): 04015114.

[6] Ji X, Wang Y, Zhang J, Okazaki T. Seismic behavior and fragility curves of replaceable steel coupling beams with slabs. Eng Struct 2017; 150: 622-35.

[7] Ji X, Liu D, Sun Y, Molina Hutt C. Seismic performance assessment of a hybrid coupled wall system with replaceable steel coupling beams versus traditional RC coupling beams. Earthquake Eng Struct Dynam 2017; 46(4):517-35.

[8] CMC. Code for Seismic Design of Buildings (GB 50011-2010). Beijing: China Architecture & Building Press; 2010 [in Chinese].

[9] CMC. Technical specification for concrete structures of tall building (JGJ 3-2010). Beijing: China Ministry of Construction; 2010 [in Chinese].

[10] Liu D. Study on Seismic Behavior and Resiliency of Novel Hybrid Coupled Wall Structures. Master Thesis. Beijing: Tsinghua University; 2017 [in Chinese].

[11] AISC. Seismic Provisions for Structural Steel Buildings (ANSI/AISC 341-10). American Institute of Steel Construction: Chicago, 2010.

[12] Naish D, Fry A, Klemencic R, Wallace J. Reinforced concrete coupling beams–Part I: testing. ACI Struct J 2013; 110(6):1057–66.

[13] OpenSEES. *Open System for Earthquake Engineering Simulation*. Pacific Earthquake Engineering Research Center. (Available from http://opensees.berkeley.edu/) [accessed on January 15, 2015].

[14] Lu X, Xie L, Guan H, Huang Y, Lu X. A shear wall element for nonlinear seismic analysis of super-tall buildings using OpenSees. Finite Elem Anal Des 2015; 98:14–25.

[15] Kent DC, Park R. Flexural members with confined concrete. ASCE J Struct Div 1971; 97(7): 1969-90.

[16] Saatcioglu M, Razvi SR. Strength and ductility of confined concrete. J Struct Eng, ASCE 1992; 118(6): 1590-07.

[17] OpenSees Wiki. Steel02 Material -- Giuffré-Menegotto-PintoModel with Isotropic Strain Hardening.http://opensees.berkeley.edu/wiki/index.php/Steel02_Material_--_Giuffr%C3%A9-Menegotto-Pinto_Model_with_Isotropic_Strain_Hardening [Accessed on January 15, 2015].

[18] Ji X, Sun Y, Qian J, Lu X. Seismic behavior and modeling of steel reinforced concrete (SRC) walls. Earthquake Eng Struct Dynam 2015; 44(6):955–72.

[19] Lu X, Li Y, Ye L, Liang Y. Application of fiber model for progressive collapse analysis of reinforced concrete frames. In: Proc 12th int conf on Computing in Civil and Building Engineering, CDROM, Beijing; Oct. 2008.

[20] ASCE/SEI. Seismic Evaluation and Retrofit of Existing Buildings (ASCE/SEI 41-06). Reston, VA: Structural Engineering Institute, 2014.

[21] SAC. Seismic ground motion parameters zonation map of China (GB 18306-2015).

Beijing: Standardization Administration of China; 2015 [in Chinese].

[22] PEER NGA-West2 Database. Pacific Earthquake Engineering Research Center, Report No. 2013/03. Berkeley, CA: University of California, Berkeley, 2013.

[23] Kaveh A, Farahmand Azar B, Hadidi A, Rezazadeh Sorochi F, Talatahari S. Performance-based seismic design of steel frames using ant colony optimization. J Constr Steel Res 2010; 66(4):566-574.

[24] Kaveh A, Zakian P. Optimal design of steel frames under seismic loading using two meta-heuristic algorithms. J Constr Steel Res 2013; 82: 111-130.

[25] Kaveh A, Bakhshpoori T, Azimi M. Seismic optimal design of 3D steel frames using cuckoo search algorithm. Stuct Design Tall Spec Build 2015; 24(3): 210-227.

[26] FEMA. Seismic performance assessment of buildings, Volume 1-Methodology, FEMA P-58-1, prepared by the Applied Technology Council for the Federal Emergency Management Agency, Washington, DC; 2012.

[27] Ji X, Xu M. Fragility research on RC shear walls and RC coupling beams. J Build Struct 2017.[in Chinese, Under review]

[28] Cai J, Bu G, Yang C, Chen Q, Zuo Z. Calculation methods for inter-story drifts of building structures. Adv Struct Eng 2014; 17(5):735-46.

[29] Yang T Y, Moehle J P, Bozorgnia Y, Zareian F, Wallace J W. Performance assessment of tall concrete core-wall building designed using two alternative approaches. Earthquake Eng Struct Dynam 2012; 41(11): 1515-31.